JAAS

ROYAL SOCIETY OF CHEMISTRY

PAPER

Cite this: *J. Anal. At. Spectrom.*, 2024, **39**, 2183

Routine measurement of high-precision potassium stable isotope compositions using a continuous-flow Neoma MC-ICPMS/MS†

Emmanuelle Albalat, Philippe Télouk and Vincent Balter *

Natural processes, from cosmochemistry to human homeostasis, can be traced by means of the mass-dependent fractionation of K isotopes because the $^{39}K/^{41}K$ ratio is characterized by a wide range of variations (*ca.* 3‰). The measurement of the $^{39}K/^{41}K$ ratio is traditionally achieved by multi-collector inductively coupled plasma mass spectrometers (MC-ICPMS), but is significantly impeded by large isobaric argide interferences on K isotopes. A new generation of MC-ICPMS equipped with a collision/reaction cell allows the quantitative elimination of argide interferences using H_2 as a reaction gas. We report on a set of high-precision K isotopic data obtained with the recently released ThermoScientific Neoma MC-ICPMS/MS equipped with a prefiltering system consisting of a double-Wien filter and a collision/reaction cell. In the low-resolution mode, the mass resolving power is *ca.* 2200, resulting in a K sensitivity of *ca.* 1000 V ppm^{-1} for ^{39}K in dry mode with an Apex Omega desolvator. This large mass revolving power allows the observation of yet undetected interferences on the high-mass shoulders of ^{39}K and ^{41}K. The interference is *ca.* 25 mV on ^{39}K and 1 mV on ^{41}K in the low-resolution mode, similar in K and blank HNO_3 (0.05 M) solutions, increases when N_2 is added in the desolvator and decreases when He is added as a collision gas. The presence of these interferences, which contribute modestly < 0.02% of the K signal, is probably the result of the formation of complex organic compounds in the collision/reaction cell. However, blank subtraction is a critical step to achieve steady and accurate analysis of the $^{39}K/^{41}K$ ratio. The overall stability of the analysis of the $^{39}K/^{41}K$ ratio is greatly improved by using a continuous-flow microFAST Isotope autosampler. A survey on the potential effects of sample-standard mismatches reveals significant offsets for matrix elements (Ca, Mg and Na), no offset for acid molarity. Regarding the effect of sample-standard concentration mismatch, we show that the amplitude of the offset is session-dependent, such that no general correction could be applied. We use the autosampler adjustable injection flow rate to correct for a concentration mismatch up to ± 30% to recover expected K isotope composition within the ± 0.05‰ uncertainty. In these conditions, short-term external precision and long-term reproducibility are 0.07‰ (2SD, $n = 500$) and 0.08‰ (2SD, $n = 66$), respectively. For validation of the overall method, we finally purified K using a single step chemical separation by ion exchange chromatography, and measured the K isotope composition of geological and biological reference materials, for which we found values similar to the literature. Our study shows that the Neoma MC-ICPMS/MS with continuous flow injection is a robust instrumentation that will contribute to expediting high-precision K isotopic measurements for various applications.

Received 7th June 2024
Accepted 1st July 2024

DOI: 10.1039/d4ja00211c

rsc.li/jaas

1 Introduction

The last few years have witnessed an increasing number of studies reporting K isotope compositions (hereafter noted as $\delta^{41}K$) for different applications, from cosmochemistry,[1–3] mantle/crust geochemistry,[4–6] hydrogeology,[7–9] environmental geochemistry,[10–12] vegetal and animal biogeochemistry[13–15] to isotope metallomics.[16–18] However, the challenge in the measurement of the $^{41}K/^{39}K$ ratio by MC-ICPMS is that argides are produced in the Ar plasma, with significant isobaric interferences of $^{40}ArH^+$ and $^{38}ArH^+$ on $^{41}K^+$ and $^{39}K^+$, respectively. Various solutions have been developed to reduce these interferences to achieve an acceptable precision of the $\delta^{41}K$ value, which are the use of a cold and dry Ar plasma,[19–24] the extra high-resolution mode (XHR) of the Neptune XT (Thermo Scientific, Bremen, Germany),[25] or the manufacturing of MC-ICPMS instruments equipped with a collision/reaction cell (CRC).

The goal of a CRC is to mitigate isobaric interferences by inducing collisions and/or reactions within an axial chamber

UMR 5276, LGL-TPE, CNRS, Ecole Normale Supérieure de Lyon, Université de Lyon 1, Lyon, France. E-mail: Vincent.Balter@ens-lyon.fr

† Electronic supplementary information (ESI) available. See DOI: https://doi.org/10.1039/d4ja00211c

that is filled with gas. Several attempts at integrating a CRC into a MC-ICPMS instrument — the IsoProbe-P (GV Instruments, Manchester, UK) with unsatisfactory external precision (*ca.* 0.2‰),[26–28] the Proteus (Thermo Scientific, Bremen, Germany) with too low sensitivity and unusual mass bias behavior,[29] and the Vienna prototype,[30] which was not commercialized — proved unfruitful for the community. However, in 2019, Nu Instruments (Wrexham, UK) commercialized the Sapphire, a dual-path CRC-MC-ICPMS allowing an external reproducibility of about 0.05‰ for routine measurements of the $^{41}K/^{39}K$ ratio at about 150 ppb.[31–35] The Sapphire has a very high sensitivity (*ca.* 2000 V ppm^{-1} for ^{39}K), is generally tolerant to matrix mismatches (with exception for Ca and HNO_3) but necessitates a close sample-standard matching of concentration (<2%) to avoid significant K isotope composition offset, thus increasing workload. To get around this difficulty, Zheng *et al.*[35] proposed a correction method, based on a general regression linear fit between the K isotope composition offset and the K intensity relative to the bracketing standard. Li *et al.*[33] investigated the CRC parameters and found that tuning the voltage of the hexapole RF alternating current can lead to a significant reduction of the K isotope composition offset.

In the present work, we use the Neoma (Thermo Scientific, Bremen, Germany) MC-ICPMS/MS to measure the $^{41}K/^{39}K$ ratio and compare the performances with the literature, notably for matrix sample-standard matching. Here, the concentration sample-standard matching is solved by using a continuous-flow microFAST Isotope autosampler allowing adjustable injection flow rate.

2 Reagents, material and sample description

All experiments were carried out in laminar flow hoods in a clean laboratory. Double-distilled acids (HNO_3, HCl, and HF), Suprapur 30% H_2O_2 (Fisher Chemical, Hampton, NH, USA) and Ultrapure water (resistivity > 18.2 MΩ cm) were used to reduce blank contaminations. Teflon beakers (Savillex™, Eden Prairie, MN, USA) were used along the procedure and Teflon columns (custom-made using retractable Teflon) filled with 210 μL of AG50W-X12 resin, hydrogen form 200–400 mesh size (Bio-Rad, Temse, Belgium) were used for K purification. We used the GA (CRPG, Nancy, France) granite and BCR-1 (USGS) basalts for geological reference materials, the IAPSO (OSIL) certified reference seawater standard, and the bovine liver SRM-1577c (NIST), whole milk BCR-380R (NRC), tuna fish ERM-CE464 (IRMM), fish protein DORM-4 (NRC), lobster hepatopancreas TORT-3 (NRC), for biological reference materials. A K solution at 1 g L^{-1} (Alfa Aesar, Ward Hill, MA, USA) diluted down to 200 ng mL^{-1}, was used as a secondary standard.

3 Method

3.1 Sample digestion and K purification

The protocols for sample digestion and K purification are fully described in Télouk *et al.*[36] and are briefly described here. Geological reference materials were digested with a mixture of concentrated HF and HNO_3 on a hot plate while biological reference materials were digested with a mixture of concentrated HNO_3 and H_2O_2 in microwave bombs. The K purification is achieved using ion-exchange chromatography using a single step procedure based on Mg purification.[37] This procedure was eventually repeated to check for the robustness of the overall protocol.

3.2 K isotope ratio measurements

All the measurements in this study were conducted on a Neoma MC-ICPMS/MS at the LGL (Laboratoire de Géologie de Lyon, Ecole Normale Supérieure de Lyon, France) with a dry plasma using an Apex Omega (Elemental Scientific Inc, Omaha, USA) desolvator. Samples, standards, and blank solutions were introduced according to a continuous flow with a microFAST Isotope (Elemental Scientific Inc, Omaha, USA) autosampler consisting of a dual-loop syringe that loads and injects solutions with rapid switching and minimal dead volume (Fig. 1). Instrument parameters are given in Table 1. The MS/MS equipment consists of a double-Wien filter and a CRC which have been extensively described in various studies.[38–40]

The sample-standard bracketing approach with a solution of SRM-3141a (NIST) at 200 ng mL^{-1} (hereafter noted K 200 ppb) as the external standard is used for correcting instrumental mass discrimination. Analyses are carried out using HNO_3 0.05 M with blank correction before measurement. The K isotopic composition is expressed as a delta value ($\delta^{41}K$, per mil, ‰) relative to SRM-3141a according to:

$$\delta^{41}K = \left[\frac{(^{41}K/^{39}K)_{sample}}{(^{41}K/^{39}K)_{standard}} - 1\right] \times 1000$$

4 Results and discussion

4.1 Measurement conditions

In the above-mentioned conditions, the K 200 ppb solution yields a typical signal of *ca.* 200 V for ^{39}K, and a blank HNO_3 (0.05 M) solution a typical signal of 600 mV for ^{39}K. The transmission of the Neoma MS/MS is thus equivalent to that of the Sapphire CRC-MC-ICPMS, which generally ranges between 0.75 and 2 V ppb^{-1}.[31,32,34,35] The blank level is, however, lower than that reported with the Sapphire CRC-MC-ICPMS that is typically 2 V for ^{39}K in HNO_3 0.05 M,[32,34,35] with the exception of the study of Chen *et al.*,[31] which reports a blank level of 350 mV. A representative peak shape of a SRM-3141a solution at 200 ppb is given in Fig. 2A, showing that the mass resolving power ($m/\Delta m$) is *ca.* 2200 in the low resolution mode (LR), well higher than that achieved with a Sapphire CRC-MC-ICPMS (*e.g.*, *ca.* 300 in the LR mode[35]). The mass resolving power is about 7000 in the medium resolution (MR, Fig. S1†). The LR mass resolution is high enough to reveal unsuspected interferences of the high mass shoulders of the ^{39}K and ^{41}K peaks (Fig. 2B). For ^{39}K, the interference is partly resolved in the LR mode (Fig. 2B), but is clearly observed in the MR mode (Fig. 2C) with a signal of *ca.*

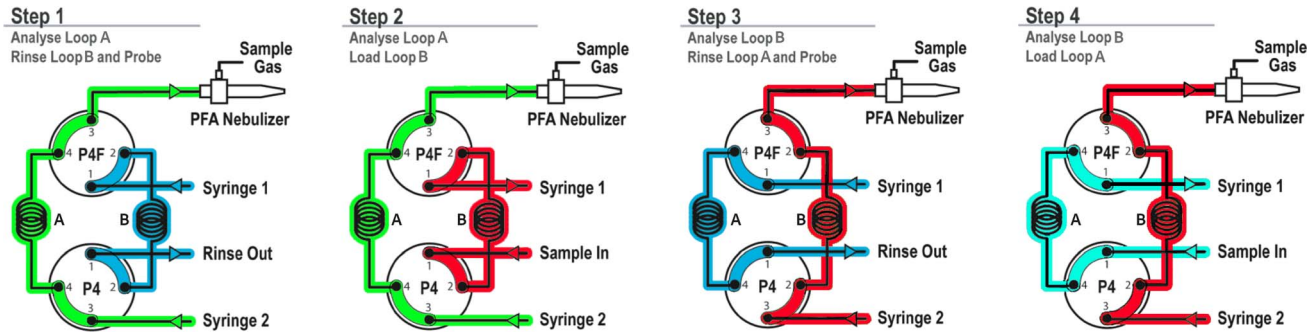

Fig. 1 Flow paths of the microFAST Isotope autosampler dual loop injection, composed of two loops (A and B), two syringes (1 and 2) and two 4-way valves (P4F and P4). The syringe 1 loads solutions while syringe 2 injects solutions at desired flow rate. During step 1, the sample solution (green) loaded in loop A is injected in the nebulizer, while the loop B is rinsed with the working solution (blue). During step 2, the sample solution (green) loaded in loop A is still injected in the nebulizer, but the loop B is now loading the new sample solution (red). During step 3, the two 4-way valves switch, such that the new sample (red) loaded in loop B is now injected, while the loop A is rinsed with the working solution (blue). During step 4, the sample solution (red) loaded in loop A is still injected in the nebulizer, but the loop B is now loading the new sample solution (cyan). Adapted from ESI©.

7 mV. This corresponds to a *ca.* 25 mV interfering signal in the LR mode, thus a significant ~5% contribution of the blank signal. For ^{41}K, the interference is resolved in the LR mode (<1 mV, Fig. 2B) and becomes too small in the MR mode to be observed (Fig. 2C). A peak shape in the LR mode reveals that residual $^{38}ArH^+$ and $^{40}ArH^+$ cannot be at the origin of the interference on $^{39}K^+$ and $^{41}K^+$, as no ^{38}Ar is detected (Fig. S2†). We then investigate different configurations to uncover the origin of these interferences and show the results as peak shapes in the MR mode to be more conveniently visualized. First, the interference is equally intense on ^{39}K in blank HNO_3 0.05 M and K 200 ppb (Fig. 3A), suggesting that it does not

Table 1 Instrument settings for K isotope analysis

Neoma MC-ICPMS/MS	
Plasma	
RF power (W)	1200
Plasma condition	Dry
Coolant Ar flow (L min^{-1})	13
Auxiliary Ar flow (L min^{-1})	0.8–1.1
Nebulizer Ar flow (L min^{-1})	1
Sampling cone	Ni Jet, $\varnothing = 1.1$ mm
Skimmer cone	Ni X-type, $\varnothing = 0.8$ mm
MS/MS	
Magnetic field	0
Electrostatic field	0
Slit aperture (%)	100
H_2 (L min^{-1})	5
He (L min^{-1})	2
Collection	
Mass resolution	~2200 (LR); ~7000 (MR)
Cup configuration	L1: ^{38}Ar ($10^{11}\Omega$); Ax: ^{39}K ($10^{10}\Omega$); H1: ^{40}Ca ($10^{11}\Omega$); H2: ^{41}K ($10^{11}\Omega$); H3: ^{42}Ca ($10^{11}\Omega$); H4: ^{43}Ca ($10^{11}\Omega$); H5: ^{44}Ca ($10^{11}\Omega$)
Sensitivity (V ppm^{-1})	~1000 (^{39}K)
Blank signal (2% HNO_3)	~600 mV (^{39}K)
Integration time (s)	4.194
Cycles	40
Apex Omega desolvator	
Ar flow (L min^{-1})	6
N_2 flow (mL min^{-1})	0
Sample uptake rate (μL min^{-1})	100

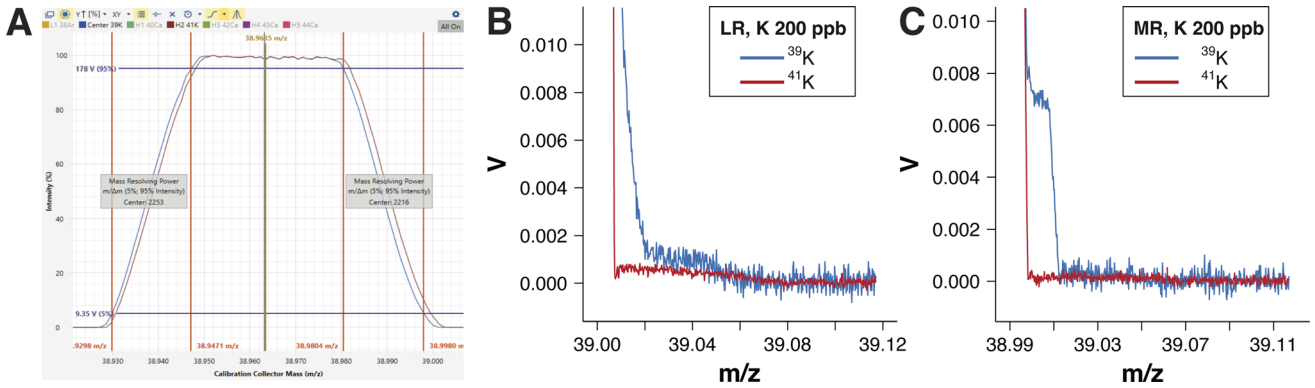

Fig. 2 (A) Peak scan in the low-resolution mode of the SRM-3141a solution at 200 ng mL^{-1} (K 200 ppb) using the set of parameters given in Table 1 showing the peak shape of the *m/z* values 39 and 41 (blue and red, respectively) with the automated calculation of the resolution (5–95% of *m/z* value 39) on the ascending edge of the peak. (B) Details of the interferences in the low-resolution mode on the high mass shoulder of the *m/z* values 39 and 41. (C) Details of the interferences in the medium-resolution mode on the high mass shoulder of the *m/z* values 39 and 41.

originate from the quality of the solutions. The presence of Ca impurities, obviously more important in K 200 ppb than in blank HNO_3 0.05 M, is observed, but Ca seems to be not affected by the interferences that affect K isotopes (Fig. S3† in the LR mode). In the blank solution, ^{40}Ca has an equal signal as ^{41}K, suggesting that potential significant $^{40}CaH^+$ isobaric interference may exist on $^{41}K^+$, thus that blank substraction is an important step to achieve accurate K isotope measurements. The relative signal of the interference on ^{39}K is slightly enhanced in H_2O and blank HCl 0.05 M solutions compared to HNO_3 (Fig. 3B), suggesting that HNO_3 is the best medium solution for measuring K isotopes. The introduction of gas significantly modifies the relative signal of the interference on K isotopes: N_2 in the Apex Omega desolvator increases that on ^{41}K (Fig. 3C), and the introduction of He in the CRC at a minimal flow of 1 mL min^{-1} decreases the interference on both ^{39}K and

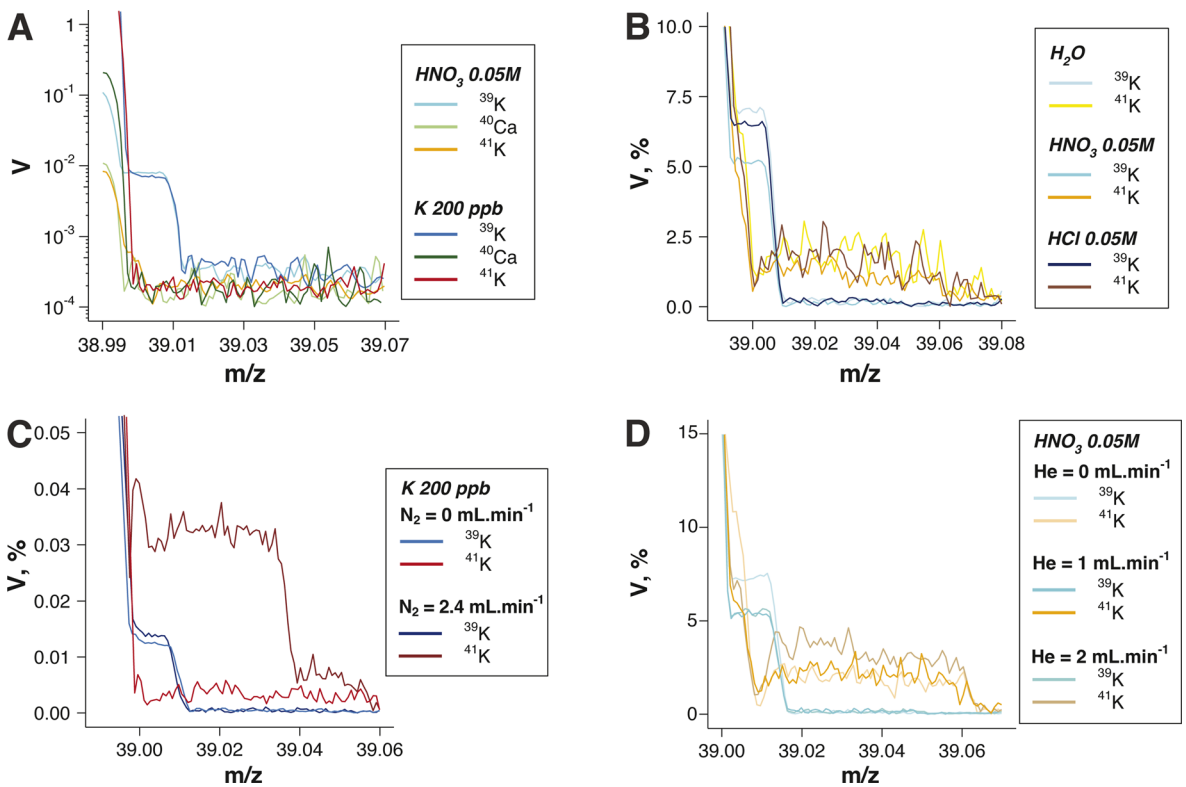

Fig. 3 (A) Details of the interferences in the medium-resolution mode on the high mass shoulder of the *m/z* values 39, 40 and 41 as a function of K concentration. Details of interferences relative intensities in the medium-resolution mode on the high mass shoulder of the *m/z* values 39 and 41: (B) as a function of the nature of the solution; (C) as a function of the presence of N_2 in the Apex Omega desolvator; (D) as a function of the presence of He in the CRC.

^{41}K, while adding an additional 1 mL min^{-1} seems to increase the relative signal of the interference on ^{41}K (Fig. 3D). Taken together, the results suggest that K isotope measurements should be achieved in a HNO_3 medium, with He in the CRC, without N_2 in the desolvator, and with blank subtraction. The precise origin of the interference on the high mass shoulders of the ^{39}K and ^{41}K peaks has not been uncovered but is likely due to the formation of organic compounds, which are known to have typical mass offsets of *ca.* 0.05 atomic mass units (amu) and manifest on the high-mass side of peaks as elevated backgrounds or, in more severe cases, as humps or shoulders. All the results in the present study are given after blank subtraction.

4.2 Sample-standard mismatches

Several analytical conditions due to mismatch between sample and standard critically affect the precision and accuracy of K isotope composition measurements using the sample-standard bracketing method. The influence of these mismatches is explored for the Neoma MS/MS and compared to the literature.

4.2.1 Effect of matrix elements. The accurate determination of isotope compositions in solutions using MC-ICP-MS requires the extraction of the analyte by ion-exchange chromatography. Nevertheless, the ion-exchange yield can differ between samples, resulting in insufficient purification of the analyte, and leading to non-spectral matrix effects due to the ionization and transmission disturbance of the analyte. In the present study, we have tested the influence of adding Ca (Fig. 4A), Mg (Fig. 4B), or Na (Fig. 4C) to the K 200 ppb solution with a K-normalized concentration ratio ranging from 2% to 4% and compared the results with the literature values. We observe offsets of the δ^{41}K value significantly outside the $\pm$ 0.05‰ range of variation for the three elements, which, however, remain in the variability observed in the literature. The results confirm that Ca is prone to generate important non-spectral matrix effects on the measurement of K isotope compositions when using a CRC-based MC-ICPMS (Fig. 4A). Of note is the positive offset of the δ^{41}K value when adding Na in the present study compared to the generally observed negative offset in the literature (Fig. 4C). This result requires further investigations using another Neoma MS/MS instrument.

4.2.2 Effect of HNO_3 concentration. In the present study, the molarity of HNO_3 is 0.05 M. We have evaluated the influence of the mismatch of the acid concentration from 0.025 M (*ca.* 0.25%) to 0.5 M (*ca.* 5%) and compared the results with the literature values (Fig. 4D). The result show no significant deviation of the δ^{41}K value within a $\pm$ 0.05‰ range of variation. It is striking to observe that such a stability can be obtained with[24,34] or without[25,36] a CRC suggesting that other analytical conditions, independent of the acid molarity mismatch, are at the origin of the observed discrepancies.[20,31,32,41] This is all the more

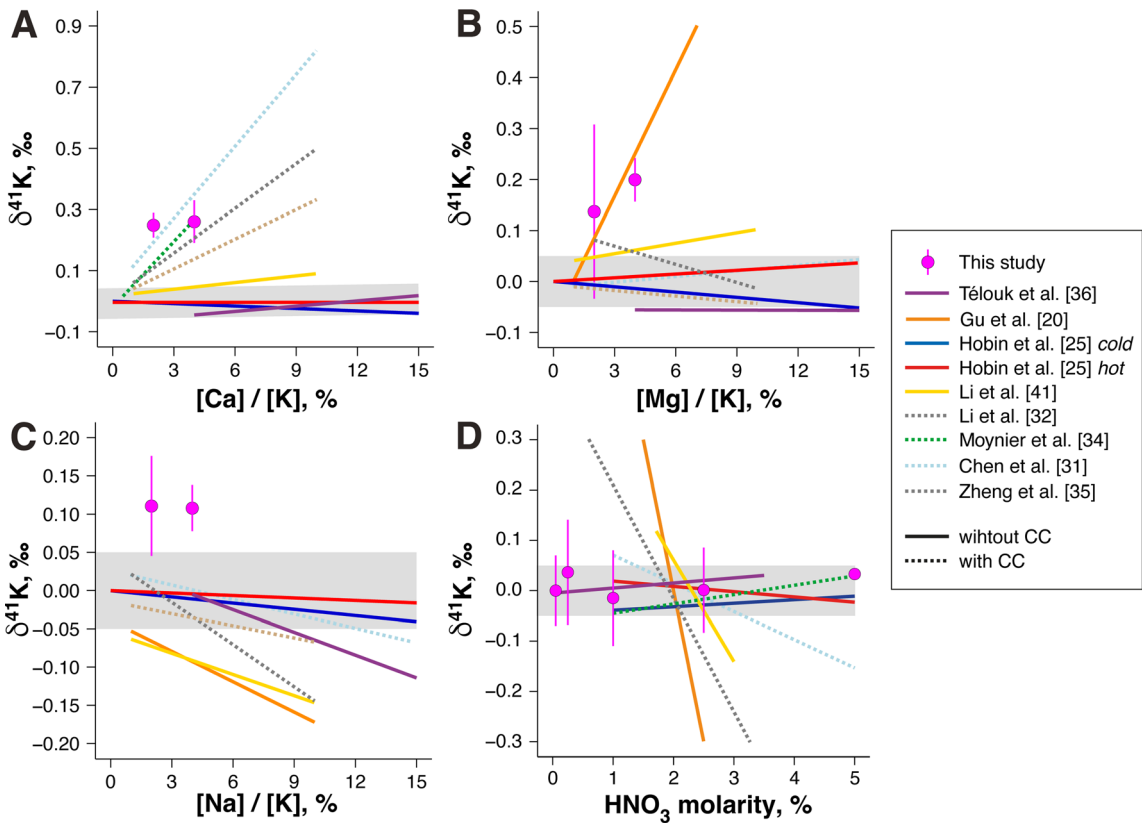

Fig. 4 Effect of sample-standard matrix mismatches on the δ^{41}K value of the sample as a function of the analyte K-normalized concentration ratio (%) for (A) Ca; (B) Na; (C) Mg; (D) HNO_3. In all cases, values from the literature are indicated, the gray area represents $\pm$ 0.05‰ from SRM-3141a, and error bars are $\pm$ 2SD.

surprising given that very different effects are obtained with the Sapphire CRC-MC-ICPMS.[31,32,34] It is noteworthy that our setup is not self aspirating.

4.2.3 Effect of K concentration. The mismatch in analyte concentration between the sample and bracketing standard has been recognized as an important factor that influences the accuracy of the δ^{41}K value. Recent research using the Sapphire CRC-MC-ICPMS[24,31–35] has indicated that this effect is even more pronounced when utilizing the low energy path, which includes the CRC, such that a linear offset of 0.02‰ is linearly produced by mismatch percent,[34] generating a debilitating increase in the workload for the operator and a significant decrease in sample throughput. Several methods have been proposed to reduce the concentration mismatch effect. A first method proposed by Zheng *et al.*[35] consists of a correction based on a regression curve between the offset of the true and measured δ^{41}K values and the concentration mismatch. A second method, proposed by Li *et al.*[33] focuses on the optimization of the CRC parameters, allowing for up to 30% improvement in the concentration mismatch. Here, we performed sample-standard concentration mismatch experiments by modifying K concentration of a K 200 ppb solution from 70% to 130%, and monitored the resulting δ^{41}K values over five different sessions during which tune parameters were left unchanged (concentration mismatch is calculated by the difference of the ^{39}K signals between the sample and the bracketing standards). Results are given in Fig. 5A. A first observation is that the slopes of the regression lines between the matching and the δ^{41}K values are positive, contrary to most of the studies performed with the Sapphire CRC-MC-ICPMS,[24,31,32,34,35] except one.[33] This suggests that the effect of concentration mismatch on the K isotope composition offset is, at first order, dependent of the instrument. However, scrutinizing the results reveals that the slopes of the regression lines are different from one session to another (Fig. 5A). All the slopes are significantly different from a general linear regression model except that of the "session #46". Therefore, this suggests that the effect of concentration mismatch on the K isotope composition offset is, at the second order, dependent of the tune parameters for a given instrument. For a similar matching value, the resulting offset of the δ^{41}K value can be very important: for example, between "session #34", which has the lowest slope, and "session #49", which has the steepest slope, the difference in the offset of the δ^{41}K value is *ca.* 0.4‰ for a matching of 80% (Fig. 5A). Overall, this suggests that no general correction method could be applied to reduce the K isotope composition offset, even for the same instrument, and that the value of the regression slope needs to be defined once the instrument is tuned.

4.2.4 Correction of the sample-standard K concentration mismatch. To correct for the K isotope composition offset due to concentration mismatch, we took advantage of the variable rate (5–1000 μL min^{-1}) of solution injection in the nebulizer of the microFAST Isotope autosampler. The nominal injection rate was setup at 100 μL min^{-1}. Increasing the injection rate leads to a negative offset of the δ^{41}K value, and *vice versa* (Fig. 5B), with an efficiency absolute value of *ca.* 2% of mismatch by 2.5 μL min^{-1} unit. After monitoring the ^{39}K signals of the sample and the bracketing standards, the corrected δ^{41}K value was obtained by simply re-analyzing the sample with the equivalence between injection rate and mismatch percent (Fig. 5B). All the δ^{41}K values of the samples, with up to ± 30% of concentration mismatch, were accordingly corrected using this method, which will benefit in the future of some improvements with an automated procedure that will record the ^{39}K signal of a sample and automatically adjust the sample injection rate to fit the ^{39}K signal of the bracketing standards.

4.3 Overall stability of the analyses

Given the set of the above-mentioned settings, the repeatability (or short-term external precision) was evaluated by repeated analyses of the SRM-3141a solution (K 200 ppb) over seven sessions which gives a value of 0.07‰ (2SD, n = 500, Table 2, Fig. 6). Repeated analyses of the Alfa Aesar solution at 200 ng mL^{-1} over four sessions give an average δ^{41}K value of 0.46 ± 0.07‰ (2SD, n = 41). Two observations are noteworthy here. The first observation is the very good stability of the instrument over a long period of time (up to forty hours, Table 2) without any

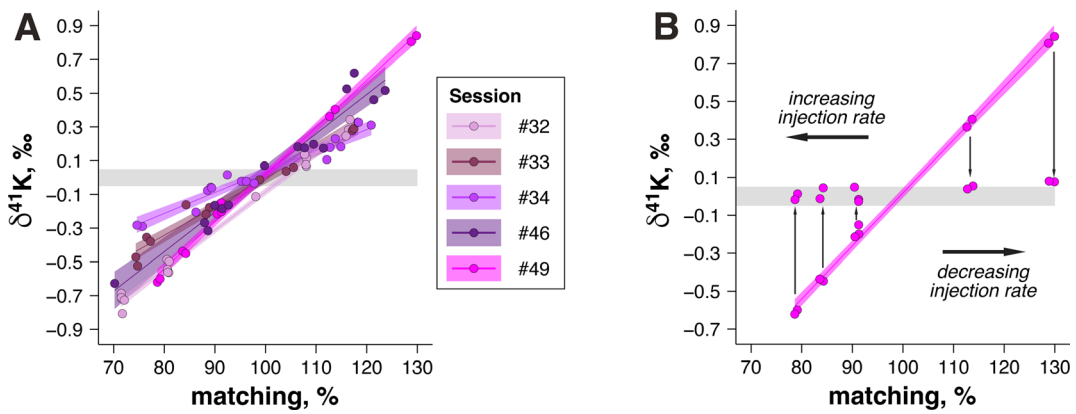

Fig. 5 (A) Effect of sample-standard concentration mismatches on the δ^{41}K value of the sample for five different sessions. (B) Correction of the effect of the sample-standard concentration mismatches for session #49. In all cases, the gray area represents ± 0.05‰ from SRM-3141a.

Table 2 K isotope composition (δ^{41}K), ^{39}K intensity, signal-to-noise ratio, number of analysis and duration without tuning instrument settings, for seven sessions illustrated in Fig. 6

Session	δ^{41}K ± 2 SD, ‰ (K 200 ppb)	^{39}K ± 2 SD, V (K 200 ppb)	^{39}K ± 2 SD, V (blank)	Signal to noise ratio, %	*n* (K 200 ppb)	*n* (blank)	Duration of analyses, h
#32	0.011 ± 0.061	159 ± 13	1.11 ± 0.03	0.69	32	49	10
#33	−0.011 ± 0.074	179 ± 50	1.26 ± 0.10	0.71	52	103	17
#34	0.010 ± 0.079	175 ± 15	1.22 ± 0.07	0.70	103	208	38
#37	0.014 ± 0.067	207 ± 42	1.45 ± 0.33	0.70	102	244	41
#44	0.008 ± 0.084	192 ± 9	0.61 ± 0.03	0.32	53	80	20
#46	−0.018 ± 0.078	212 ± 9	0.64 ± 0.09	0.30	72	182	40
#49	0.001 ± 0.074	213 ± 10	0.46 ± 0.12	0.22	86	273	45

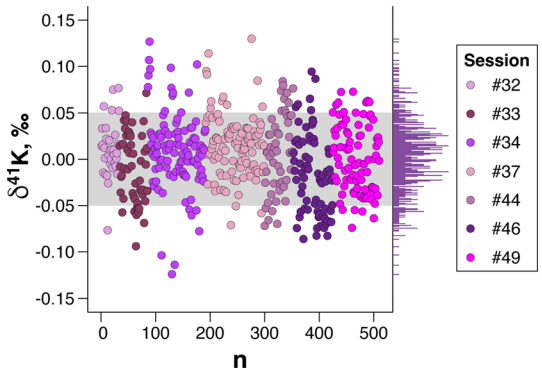

Fig. 6 Stability of the δ^{41}K value of the SRM-3141a solution at 200 ng mL^{-1} (K 200 ppb) sample over seven different sessions. The gray area represents ± 0.05‰ from SRM-3141a.

tuning. Progressive optimization of the instrument tuning parameters led to improved transmission while reducing the signal-to-noise ratio over successive sessions (Table 2). The second observation is the high throughput achieved using the continuous-flow microFAST Isotope autosampler: for example, during a 40 hour single session, about one hundred samples are measured with as many standards and twice as many blanks, corresponding to *ca.* ten analyses per hour. The intermediate precision, or long-term external reproducibility was evaluated from the uncertainties measured on the reference materials, which gives a value of 0.08‰ (2SD, $n = 66$).

4.4 K isotope compositions of biological and geological reference materials

For validation of the overall method, we finally measured the K isotope composition of geological and biological reference materials (RM). The reference material measured in the present study agree well with those of the literature (Table 3). For all the RM, we processed ion-exchange chromatography K purification once or twice and found no significant different resulting δ^{41}K values (Table S1†), suggesting that the overall protocol is robust enough using a single step chemistry opening perspectives for online K purification and isotope analyses.

5 Conclusion

We report on a set of high-precision K isotopic data obtained with the recently released ThermoScientific Neoma MC-ICPMS/MS. The large mass revolving power allows the observation of yet undetected interferences on the high-mass shoulders of ^{39}K and ^{41}K, which are probably the result of the formation of complex organic compounds in the collision/reaction cell. Blank subtraction allows to achieve steady and accurate analyses of the K isotope compositions. Using a continuous-flow microFAST Isotope autosampler, which has configurable injection flow rates to correct for concentration mismatches, significantly improves throughput and the overall stability of the K isotope composition measurements.

Table 3 K isotope composition (δ^{41}K) of the CRM measured in the present study. *n** and *n* refer to the number of replicates and the number of analyses, respectively. Data from the literature are indicated

This study					Literature	
RM	Nature	δ^{41}K ± 2 SD, ‰	*n**	*n*	δ^{41}K ± 2 SD, ‰	Reference
BCR-1	Basalt	−0.37 ± 0.12	2	5	−0.43 ± 0.06	19, 21, 23, 25, 31 and 36
GA	Granite	−0.46 ± 0.07	2	9	−0.46 ± 0.08	23, 34 and 36
SRM-1577c	Bovine liver	0.16 ± 0.04	2	7	0.15 ± 0.00	14 and 36
DORM-4	Fish protein	−0.24 ± 0.07	2	6	−0.24	36
BCR-383	Green beans	−0.82 ± 0.11	3	10	−0.83 ± 0.03	14 and 36
IAPSO	Seawater	0.09 ± 0.18	2	7	0.09 ± 0.11	14, 32 and 36
ERM-CE464	Tuna fish	0.36 ± 0.03	2	10	0.33 ± 0.09	14, 36 and 42
TORT-3	Lobster hepatopancreas	−0.26 ± 0.02	2	6	−0.30 ± 0.03	25 and 36
BCR-380	Whole milk	0.05 ± 0.10	2	6	0.07 ± 0.00	14 and 36

Data availability

The data supporting this article have been included in the main text or as part of the ESI.†

Conflicts of interest

The authors do not have any conflicts of interest to declare.

Acknowledgements

The authors thank two anonymous reviewers for their comments and L. Delette for helping in the isotopic measurements, the staff at Elemental Scientific Inc for providing a microFAST autosampler and technical support as part of the formal collaboration with ENS-Lyon. This project has received financial support from the CNRS through the MITI interdisciplinary programs.

References

1 Y. Hu, F. Moynier, W. Dai, M. Paquet, T. Yokoyama, Y. Abe, J. Aléon, C. M. O. Alexander, S. Amari, Y. Amelin, K. Bajo, M. Bizzarro, A. Bouvier, R. W. Carlson, M. Chaussidon, B.-G. Choi, N. Dauphas, A. M. Davis, T. Di Rocco, W. Fujiya, R. Fukai, I. Gautam, M. K. Haba, Y. Hibiya, H. Hidaka, H. Homma, P. Hoppe, G. R. Huss, K. Ichida, T. Iizuka, T. R. Ireland, A. Ishikawa, S. Itoh, N. Kawasaki, N. T. Kita, K. Kitajima, T. Kleine, S. Komatani, A. N. Krot, M.-C. Liu, Y. Masuda, M. Morita, K. Motomura, I. Nakai, K. Nagashima, D. Nesvorný, A. Nguyen, L. Nittler, M. Onose, A. Pack, C. Park, L. Piani, L. Qin, S. S. Russell, N. Sakamoto, M. Schönbächler, L. Tafla, H. Tang, K. Terada, Y. Terada, T. Usui, S. Wada, M. Wadhwa, R. J. Walker, K. Yamashita, Q.-Z. Yin, S. Yoneda, E. D. Young, H. Yui, A.-C. Zhang, T. Nakamura, H. Naraoka, T. Noguchi, R. Okazaki, K. Sakamoto, H. Yabuta, M. Abe, A. Miyazaki, A. Nakato, M. Nishimura, T. Okada, T. Yada, K. Yogata, S. Nakazawa, T. Saiki, S. Tanaka, F. Terui, Y. Tsuda, S. Watanabe, M. Yoshikawa, S. Tachibana and H. Yurimoto, *Icarus*, 2024, **409**, 115884.
2 Y. Ku and S. B. Jacobsen, *Sci. Adv.*, 2020, **6**, eabd0511.
3 Y. Hu, F. Moynier and M. Bizzarro, *Nat. Commun.*, 2022, **13**, 7669.
4 W. Li, L. A. Coogan, K. Wang, Y. Takahashi, M. Shakouri, Y. Hu and X.-M. Liu, *Earth Planet. Sci. Lett.*, 2024, **625**, 118448.
5 C. A. Parendo, S. B. Jacobsen and T. Plank, *Geochim. Cosmochim. Acta*, 2022, **337**, 166–181.
6 K. Wang and D. A. Ionov, *Earth Planet. Sci. Lett.*, 2023, **619**, 118315.
7 K. Wang, H. G. Close, B. Tuller-Ross and H. Chen, *ACS Earth Space Chem.*, 2020, **4**, 1010–1017.
8 T.-T. Ji, X.-W. Jiang, G. Han, X. Li, L. Wan, Z.-Z. Wang, H. Guo and Z. Jin, *Earth Planet. Sci. Lett.*, 2024, **626**, 118526.
9 J. I. Taotao and J. Xiaowei, *Hydrogeol. Eng. Geol.*, 2023, **50**, 10–19.
10 R. Qu, G. Han and J. Zeng, *J. Cleaner Prod.*, 2024, **435**, 140574.
11 R. Qu and G. Han, *Environ. Chem. Lett.*, 2023, **21**, 41–45.
12 W. Li, X.-M. Liu, Y. Hu, F.-Z. Teng and Y. Hu, *Geochim. Cosmochim. Acta*, 2021, **304**, 160–177.
13 M.-Y. He, T. X. Ren, Z. D. Jin, L. Deng, H. J. Liu, Y. Y. Cheng, Z. Y. Li, X. X. Liu, Y. Yang and H. Chang, *Spectrochim. Acta, Part B*, 2023, **209**, 106781.
14 T. Tacail, J. Lewis, M. Clauss, C. D. Coath, R. Evershed, E. Albalat, T. R. Elliott and T. Tütken, *Metallomics*, 2023, **15**, mfad065.
15 R. Qu and G. Han, *J. Geophys. Res.: Biogeosci.*, 2022, **127**, e2021JG006682.
16 M.-M. Cui, F. Moynier, B.-X. Su, W. Dai, Y. Hu, D. Rigoussen, B. Mahan and M. Le Borgne, *Metallomics*, 2023, **15**, mfad033.
17 K. Schilling, H. Chen, R. A. Glabonjat, S. Debernardi, O. Blyuss, A. Navas-Acien, A. N. Halliday and T. Crnogorac-Jurcevic, *Front. Endocrinol.*, 2024, **15**, 1332895.
18 J. A. Higgins, D. S. Ramos, S. Gili, C. Spetea, S. Kanoski, D. Ha, A. A. McDonough and J. H. Youn, *Front. Physiol.*, 2022, **13**, 1016242.
19 H. Chen, Z. Tian, B. Tuller-Ross, R. L. Korotev and K. Wang, *J. Anal. At. Spectrom.*, 2019, **34**, 160–171.
20 H.-O. Gu and H. Sun, *J. Anal. At. Spectrom.*, 2021, **36**, 2545–2552.
21 Y. Hu, X.-Y. Chen, Y.-K. Xu and F.-Z. Teng, *Chem. Geol.*, 2018, **493**, 100–108.
22 L. E. Morgan, D. P. S. Ramos, B. Davidheiser-Kroll, J. Faithfull, N. S. Lloyd, R. M. Ellam and J. A. Higgins, *J. Anal. At. Spectrom.*, 2018, **33**, 175–186.
23 Y.-K. Xu, Y. Hu, X.-Y. Chen, T.-Y. Huang, R. S. Sletten, D. Zhu and F.-Z. Teng, *Chem. Geol.*, 2019, **513**, 101–107.
24 S. An, X. Luo and W. Li, *Rapid Commun. Mass Spectrom.*, 2022, **36**, e9289.
25 K. Hobin, M. Costas Rodríguez and F. Vanhaecke, *Anal. Chem.*, 2021, **93**, 8881–8888.
26 F. M. Richter, E. Bruce Watson, M. Chaussidon, R. Mendybaev, J. N. Christensen and L. Qiu, *Geochim. Cosmochim. Acta*, 2014, **138**, 136–145.
27 W. Li, B. L. Beard and S. Li, *J. Anal. At. Spectrom.*, 2016, **31**, 1023–1029.
28 K. Wang and S. B. Jacobsen, *Geochim. Cosmochim. Acta*, 2016, **178**, 223–232.
29 D. Bevan, C. D. Coath, J. Lewis, J. Schwieters, N. Lloyd, G. Craig, H. Wehrs and T. Elliott, *J. Anal. At. Spectrom.*, 2021, **36**, 917–931.
30 G. Craig, H. Wehrs, D. G. Bevan, M. Pfeifer, J. Lewis, C. D. Coath, T. Elliott, C. Huang, N. S. Lloyd and J. B. Schwieters, *Anal. Chem.*, 2021, **93**, 10519–10527.
31 H. Chen, N. J. Saunders, M. Jerram and A. N. Halliday, *Chem. Geol.*, 2021, **578**, 120281.
32 W. Li, M. Cui, Q. Pan, J. Wang, B. Gao, S. Liu, M. Yuan, B. Su, Y. Zhao, F.-Z. Teng and G. Han, *Sci. China: Earth Sci.*, 2022, **65**, 1510–1521.
33 W. Li, Y. Zhao, B. Su, B. Gao, J. Wang and S. Liu, *J. Anal. At. Spectrom.*, 2023, **38**, 603–608.

34 F. Moynier, Y. Hu, K. Wang, Y. Zhao, Y. Gérard, Z. Deng, J. Moureau, W. Li, J. I. Simon and F.-Z. Teng, *Chem. Geol.*, 2021, **571**, 120144.
35 X.-Y. Zheng, X.-Y. Chen, W. Ding, Y. Zhang, S. Charin and Y. Gérard, *J. Anal. At. Spectrom.*, 2022, **37**, 1273–1287.
36 P. Télouk, E. Albalat, T. Tacail, F. Arnaud-Godet and V. Balter, *J. Anal. At. Spectrom.*, 2022, **37**, 1259–1264.
37 S. Le Goff, E. Albalat, A. Dosseto, J.-P. Godin and V. Balter, *Rapid Commun. Mass Spectrom.*, 2021, **35**, e9074.
38 N. Dauphas, T. Hopp, G. Craig, Z. J. Zhang, M. C. Valdes, P. R. Heck, B. L. A. Charlier, E. A. Bell, T. M. Harrison, A. M. Davis, L. Dussubieux, P. R. Williams, M. J. Krawczynski, C. Bouman, N. S. Lloyd, D. Tollstrup and J. B. Schwieters, *J. Anal. At. Spectrom.*, 2022, **37**, 2420–2441.
39 P. Télouk, E. Albalat, B. Bourdon, F. Albarède and V. Balter, *J. Anal. At. Spectrom.*, 2023, **38**, 1973–1983.
40 P. Télouk and V. Balter, *J. Anal. At. Spectrom.*, 2024, **39**, 879–887.
41 X. Li, G. Han, Q. Zhang and Z. Miao, *J. Anal. At. Spectrom.*, 2020, **35**, 1330–1339.
42 F. Moynier, Y. Hu, W. Dai, E. Kubik, B. Mahan and J. Moureau, *J. Anal. At. Spectrom.*, 2021, **36**, 2444–2448.